Precise Determination of the Threshold Diameter for a Single-Walled Carbon Nanotube To Collapse

Maoshuai He,[†,‡,#,*] Jichen Dong,[§,∥,#] Kaili Zhang,[§] Feng Ding,[∥,*] Hua Jiang,[⊥] Annick Loiseau,[†] Juha Lehtonen,[‡] and Esko I. Kauppinen[⊥]

[†]Laboratoire d'Étude des Microstructures, ONERA-CNRS, BP 72, 92322 Châtillon CEDEX, France, [‡]Department of Biotechnology and Chemical Technology, Aalto University School of Chemical Technology, P.O. Box 16100, FI-00076 Aalto, Finland, [§]Department of Mechanical and Biomedical Engineering, City University of Hong Kong, 83 Tat Chee Avenue, Kowloon, Hong Kong, [∥]Institute of Textiles and Clothing, Hong Kong Polytechnic University, Kowloon, Hong Kong, and [⊥]Department of Applied Physics and Center for New Materials, Aalto University School of Science, P.O. Box 15100, FI-00076 Aalto, Finland

ABSTRACT Closed-edged bilayer graphene nanoribbons were formed by the spontaneous collapse of large-diameter single-walled carbon nanotubes (SWNTs) grown on gold nanoparticles by chemical vapor deposition. Such bilayer graphene nanoribbons could adopt different stacking configurations, such as AB-stacking or stacking order with any rotation angle, correlated with the chiral angles of their parent rounded SWNTs. On the basis of the electron diffraction characterizations on a good number of collapsed and uncollapsed SWNTs, the threshold diameter for SWNTs to collapse was precisely determined to be 5.1 nm, independent of the chiral angle of the SWNTs. The determination is consistent with that calculated by both classical adaptive intermolecular reactive empirical bond order force field and density functional theory after having taken the stacking effect and thermal fluctuation into account.

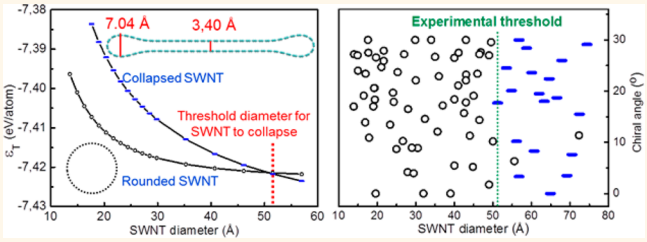

KEYWORDS: closed-edged bilayer graphene nanoribbon · large-diameter single-walled carbon nanotube · collapse · gold catalyst · chemical vapor deposition

Closed-edged graphene nanoribbons[1−10] are emerging as a new analogue of graphene nanoribbons with defined edge structures, which exhibit interesting mechanical[1,5,7] and electrical properties,[8,9] thus holding promise as building blocks in high-performance nanoelectronics. Such kind of graphene nanoribbons with only two layers, namely closed-edged bilayer graphene nanoribbons (CE-BL-GNRs) can be formed by the collapse of large-diameter multiwalled carbon nanotubes after extracting inner tubes by sonication.[9] Different from the sonication-induced extraction processes which usually generate relatively wide CE-BL-GNRs,[9] the spontaneous collapse of large-diameter single-walled carbon nanotubes (SWNTs) provides an efficient and promising strategy for achieving narrow CE-BL-GNRs.[1,2] It has been widely accepted that a SWNT collapses spontaneously when its diameter exceeds a threshold,[1,2,4,11−17] which is defined as the threshold diameter for SWNT to collapse (D_T). However, the reported D_T determined mainly by transmission electron microscopy (TEM) images differs from each other and has been a focus of controversy. For example, the D_T for SWNTs reported by Motta *et al.*[1] is 4.6 nm, in contrast with 2.6 nm claimed by Zhang *et al.*[2] A similar situation exists for the calculated or simulated threshold diameters, where D_T ranges from 0.9 to 6.9 nm based on different computational methods.[2,4,11−17] Consequently, this creates a research challenge for the reliable and precise determination of D_T.

The discrepancy in D_T values is partly attributed to the lack of large-diameter SWNTs in most carbon nanotube products. Although great progress has been made in chemical vapor deposition (CVD) growth of SWNTs,[18−24] studies on growing large-diameter SWNTs,[21,23,25] especially collapsed ones have been scarce, because most catalyst nanoparticles with increasing diameter tend to nucleate double-walled carbon nanotubes[26] or even multiwalled carbon nanotubes[23,27] instead of SWNTs. Even though large-diameter or few collapsed SWNTs were observed in some experiments,[1,2,21] the SWNTs usually

* Address correspondence to hemaoshuai@gmail.com, feng.ding@polyu.edu.hk.

Received for review August 1, 2014 and accepted August 17, 2014.

Published online August 18, 2014
10.1021/nn5042812

exist in bundles[1,2] or lie on substrate[21] and need to be transferred to a grid for TEM characterizations. The transfer processes[9] or the interactions of the SWNTS with the support[28] might cause structural deformation and complicate the determination of D_T. To lift the hurdle for TEM characterizations, direct growth of individual, free-standing SWNTs with large diameters is highly preferred.

Besides the difficulties in growing free-standing SWNTs with large diameters, it is also hard to judge whether a carbon nanotube collapses or not by its TEM image,[1−3] as the TEM image is only a two-dimensional projection of an object. By imaging the open-edge of the tubes[1,2] or sample rotation studies,[3] it is possible to confirm the collapse of the tubes. Unfortunately, these strategies are tedious and not efficient. Just recently, Zhang *et al.*[2] proposed to distinguish the collapsed tubes from uncollapsed ones based on the observed kinks on the carbon nanotube walls. Nevertheless, using kinks as indicators of collapsed SWNTs is questionable, as has been suggested by molecular dynamic simulations that kinks only lead to the local deformation of tubes.[29] Consequently, it is necessary to develop an efficient and reliable technique to distinguish collapsed SWNTs from uncollapsed ones. More importantly, the stacking order of the CE-BL-GNRs, which is interesting for studying their stability[30] and the effect of interlayer lattice registry,[4,15] has been lacking in previous experimental work.

In the work reported here, we will first demonstrate the CVD synthesis of free-standing, large-diameter SWNTs on Au nanoparticles. A number of SWNTs collapse spontaneously to from CE-BL-GNRs due to their ultralarge diameters. The stacking order of CE-BL-GNRs will be evaluated by analyzing their nanobeam electron diffraction (ED) patterns. On the basis of the extensive ED characterizations on the rounded and collapsed SWNTs, the threshold diameter, D_T, of the SWNTs to collapse will be precisely determined. Finally, the observed threshold diameter will be explained by the theoretical calculation which counts the stacking order effect and the thermal fluctuation.

RESULTS AND DISCUSSION

Isolated, free-standing SWNTs were grown by CVD on Au nanoparticles (about 10 nm) which had been dispersed on a Si_3N_4 TEM grid (DuraSiN mesh). Figure 1a shows an overview of the as-received Au nanoparticles. The schematic illustration of the SWNT growth process is shown in Figure 1b. Si_3N_4 grid supported Au nanoparticles were first annealed in open air for 2 h before being subjected to CVD growth in the presence of methane at 950 °C. The air calcination reduces the particle size owing to the particle evaporation,[31] and is necessary to activate the Au nanoparticles for growing carbon nanotubes.[32] Figure 1c depicts a typical TEM image of an individual, free-standing SWNT grown on

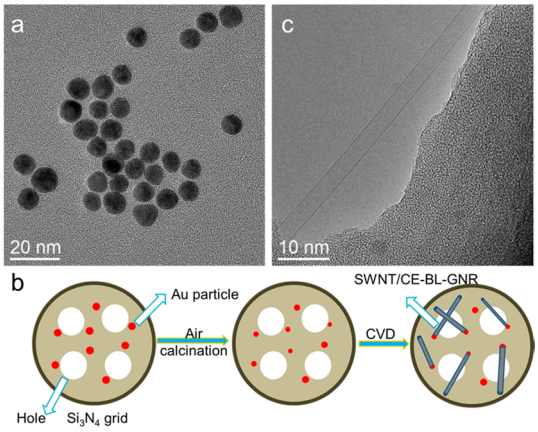

Figure 1. (a) TEM overview of as-received 10 nm Au nanoparticles. (b) Schematic illustration for synthesizing individual, free-standing SWNTs or CE-BL-GNRs with large diameters by CVD. (c) A typical TEM image of an isolated SWNT grown on Au catalyst predispersed on a Si_3N_4 TEM grid.

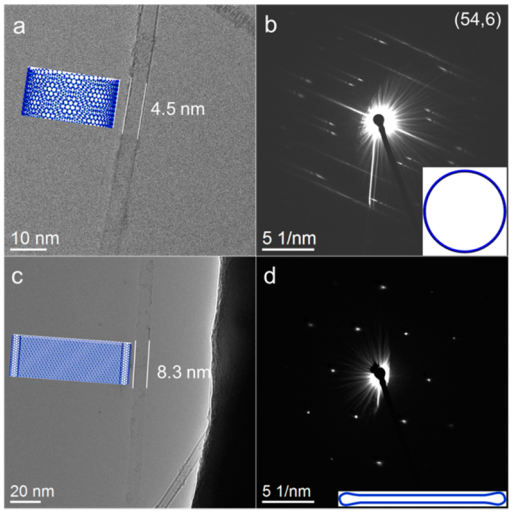

Figure 2. . (a) TEM image of an individual, rounded SWNT and (b) its ED pattern. The chirality of the SWNT is assigned as (54, 6) by analyzing its ED pattern. (c) TEM image of a CE-BL-GNR from a collapsed SWNT and (d) its ED pattern. The insets show the configurations of the uncollapsed and collapsed SWNTs.

the Au catalyst. Different from double-walled or multiwalled carbon nanotubes grown on large-diameter transition-metal nanoparticles,[23,26,27] carbon nanotubes grown on Au nanoparticles are mainly single-walled. The growth of SWNTs instead of multiwalled carbon nanotubes on large Au nanoparticles is related to the relatively low carbon solubility in the Au particles,[33] which is of great importance for inhibiting extra wall formation during the tube nucleation process.

Figure 2 panels a and b present a TEM image of one SWNT and its corresponding ED pattern, respectively. The ED pattern of the SWNT displays a strong equatorial oscillation and nonequatorial layer-lines, which are described by Bessel functions with certain orders

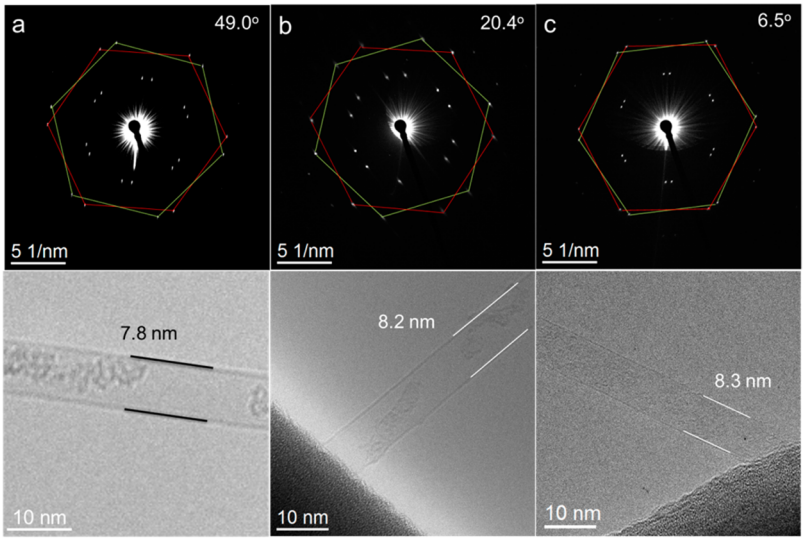

Figure 3. ED patterns of three CE-BL-GNRs formed from collapsed SWNTs, and their corresponding TEM images. Both the alignment angles and the widths of the CE-BL-GNRs are indicated.

associated with its chiral indices.[34−36] As a consequence of the curvature and the finite lateral size of the SWNT, the spots are elongated and their intensities fade away toward the exterior (Figure S1, Supporting Information). From its diffraction pattern, the chirality (*n*, *m*) of the SWNT is assigned as (54, 6), denoting a metallic SWNT with a chiral angle of 5.2° and a diameter of 4.5 nm. The calculated diameter agrees with the diameter measured directly from its TEM image (Figure 2a). The SWNT is thus believed to be uncollapsed and adopt a cylindrical configuration (Inset of Figure 2b). Extensive ED characterizations on SWNTs have been performed, revealing that all SWNTs smaller than 5.1 nm exhibit typical diffraction features of rounded, uncollapsed SWNTs. The findings are in agreement with our previous ED characterization results on Fe-grown SWNTs with diameters smaller than 4.6 nm,[24] where no tube collapse has ever been observed. Besides straight, well-structured SWNTs, SWNTs with kinks (Figure S2, Supporting Information) or folds (Figure S3, Supporting Information) were also observed frequently even for SWNTs with relatively small diameters. As indicated by the ED patterns of SWNTs shown in Figure S2d and Figure S3c, the structures of the straight parts of a SWNT remained inflated and the local deformations would not induce the collapse of the entire SWNT.[29] Therefore, using such local deformations in SWNTs as indicators of collapse[2] could be misleading. Indeed, when applying tensile load at high temperatures, the kinks in carbon nanotubes were reported to motion along the tubes[37] without collapsing the targeted tubes.

Besides a cylindrical configuration of SWNTs, fully collapsed SWNTs, that is, CE-BL-GNRs with a "dog bone" structure,[1] of which the cross-section view is composed of two highly strained circular edges bridged by a flat middle section are also energetically favorable.[2,15] Figure 2c shows a TEM image of a CE-BL-GNR with a width of 8.3 nm, the projection of which looks like that of a round SWNT. However, its ED pattern (Figure 2d) differs greatly from that of a inflated SWNT. In addition to the equatorial lines vanishing and dot elongating (Figure S4, Supporting Information), hexagonal patterns with spacings and symmetry consistent with those of graphene[38,39] were observed, indicating that the SWNT is fully collapsed forming a CE-BL-GNR (Insets of Figure 2c and 2d). On the basis of the linear relationships between measured width (W) and the diameter (D) of the original cylindrical SWNT before collapse: $W = 1.536 \times D - 0.372$ (the formula will be discussed later), the diameter of the SWNT when in the rounded state is calculated to be 5.6 nm. In addition, from the ribbon orientation and its ED pattern, it is deduced that the formed CE-BL-GNR is AB-stacked with an alignment angle $\alpha = 60°$. Consequently, it is supposed that the CE-BL-GNR is formed from the collapse of an armchair SWNT, say, a (41, 41) tube. The diameter of the rounded, parental SWNT for the CE-BL-GNR is believed to match the diameter of the catalytic Au nanoparticle, nucleating the large-diameter SWNT by a tangential mode.

CE-BL-GNRs with different stacking orders were detected based on ED pattern analysis. Figure 3 presents TEM images of three nanoribbons and their corresponding ED patterns. The three CE-BL-GNRs have widths of 7.8, 8.2, and 8.3 nm, respectively. By converting the widths of collapsed SWNTs to the diameters of their uncollapsed states, diameters of 5.3, 5.6, and 5.6 nm were calculated respectively for their rounded states. Different from AB stacked CE-BL-GNR, each diffraction pattern in Figure 3a−c presents two sets of hexagons (as schematically illustrated in red and green), resulting from the diffraction from the front side and the back side of the graphene nanoribbons,

respectively. The two hexagons are rotated by α (α/2 is the chiral angle of its parent SWNT), which were respectively determined to be 49.0° (Figure 3a), 20.4° (Figure 3b), and 6.5°(Figure 3c). Although the graphene layers may undergo a rotation to reach a local energy minimum because of the lattice registry effect,[4,15] the rotation (if there is some) is minor (Figure S5 Supporting Information) and the above CE-BL-GNRs were formed from collapse of SWNTs with the original chiral angles near 24.5°, 10.2°, and 3.3°, respectively. Therefore, by collapsing large-diameter SWNTs, it is possible to obtain CE-BL-GNRs with different stacking orders.

On the basis of the ED pattern analysis from abundant rounded and collapsed SWNTs, the relationship between the calculated diameters of cylindrical SWNTs from their ED-defined chiral index and their chiral angles is plotted in Figure 4 (the open circles in black). A similar association between the diameters and chiral angles of parent cylindrical SWNTs which were calculated from the widths and ED patterns of the CE-BL-GNRs is also shown (the solid lines in blue). No collapse of SWNT occurs for free-standing SWNTs smaller than 5.1 nm, suggesting that the threshold diameter, D_T, for SWNT collapse is 5.1 nm and is independent of SWNT chiral angles. It is noted that a SWNT with a diameter larger than 5.1 nm does not necessarily collapse. Figure S6 (Supporting Information) presents TEM images of two SWNTs with diameters of 5.6 and 7.2 nm, respectively. As suggested by their ED patterns, both the SWNTs still preserve their inflated configurations. Indeed, an uncollapsed large-diameter SWNT was also occasionally observed in some previous work.[23] The reasons for the "unusual" collapse behaviors of some large-diameter SWNTs will be discussed later.

To explain the collapse of SWNTs observed in our experiments, theoretical calculations based on both classical adaptive intermolecular reactive empirical bond order (AIREBO) force field[40] and density functional theory (DFT) were implemented. Details of the calculation information were given in the Methods section. Whether an SWNT collapses or not mainly depends on its diameter-related energy balance between the surface energy (van der Waals (vdW) interaction between the adhering layers and the elastic energy (curvature energy). Figures S7 and S8 (Supporting Information) present the curvature energy and vdW attractive energy for SWNTs with different diameters, respectively. Figure 5a shows the average total energy (ε_T) of rounded and collapsed armchair SWNTs with different diameters. Obviously, with the increase of diameter, the stability of armchair SWNTs can be divided into three stages. When the diameter is smaller than 1.76 nm, only round shape armchair SWNTs exist. For diameters between 1.76 and 4.07 nm, though the total energy of collapsed armchair SWNTs is higher than that of the corresponding round ones, the collapsed SWNTs can be metastable due to the small energy difference. The most stable state transits from the round shape to the collapsed shape at a threshold diameter of about 4.07 nm. Similar phenomenon is also observed in zigzag SWNTs (Figure 5b), except for the slight difference in the threshold diameters for state transition. The insets in Figure 5 panels a and b illustrate the optimized structure of collapsed SWNTs. The distance between two opposite walls (3.4 Å) is actually the interlayer distance in graphite, which is in agreement with the wall distance observed experimentally from a twisted CE-BL-GNR (Figure S9, Supporting Information). Moreover, the height of the highly strained edges nearly equals the diameter of C_{60} (7 Å), indicating the validity of the used force field.

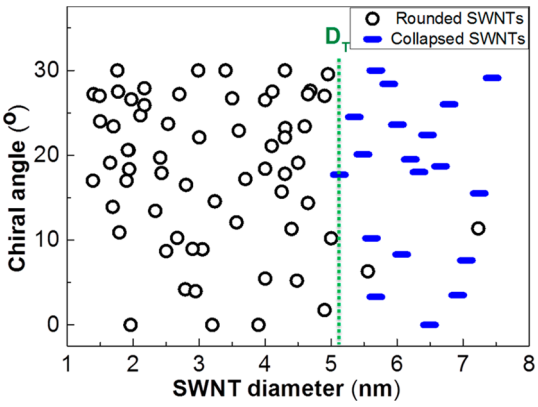

Figure 4. Correlations between calculated SWNT diameters and their corresponding chiral angles. All the diameters of the parent SWNTs for CE-BL-GNRs were calculated based on the formula: $W = 1.536 \times D - 0.372$.

Supporting Information Table S1 shows a summary of D_T obtained from calculations using the second generation reactive empirical bond order potential (Brenner or REBO potential) and its derivatives (AIREBO) in the literature. It can be seen that the main difference between these calculations lies in the description of long-range atomic interaction or the vdW interaction. A stronger vdW interaction (refs 2 and11 compared to refs 4 and16) gives a small D_T, indicating the critical role of the vdW interaction in SWNT collapse.

It should be noted that the calculated D_T for SWNTs to collapse by comparing the optimized energies is ~1.0 nm smaller than the experimental measured number. This could be attributed to two unconsidered effects: (i) the overestimation of vdW interaction between the graphene walls of collapsed SWNTs by neglecting the stacking effect in the AIREBO potential and (ii) the thermal fluctuation at finite temperature, each of which could reduce the vdW interaction between graphene layers and therefore lead to a large D_T.

The traditional Lennard-Jones (12−6) potential has its intrinsic drawback that the vdW interaction between graphene layers is not sensitive to the stacking patterns (the vdW energy difference between AB

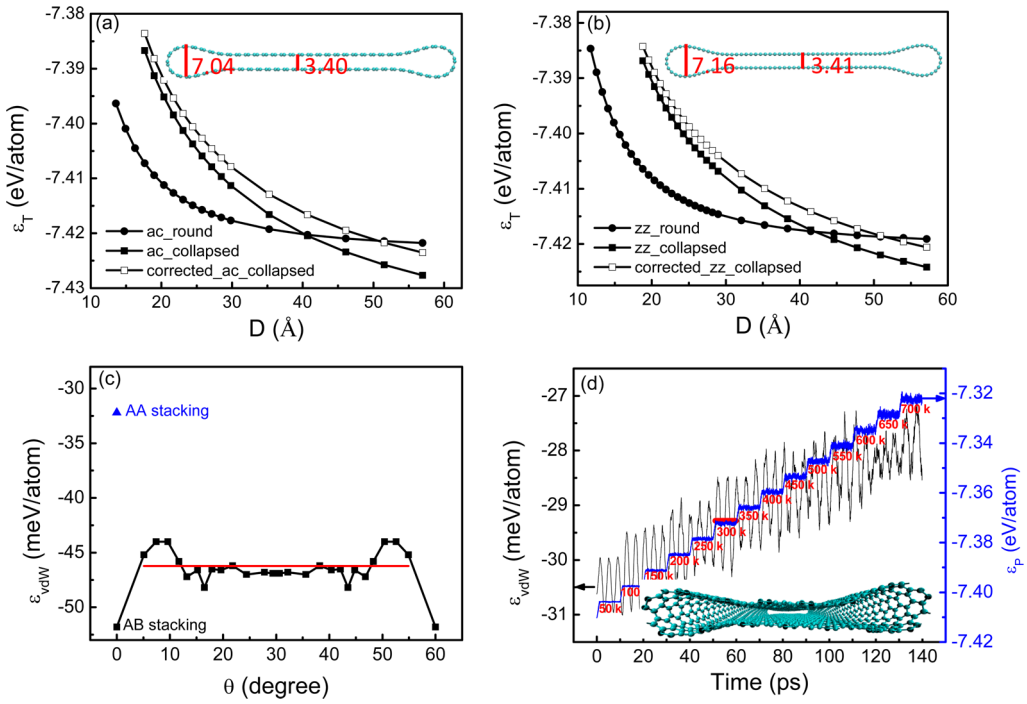

Figure 5. Total energy (black solid symbol lines) and corrected total energy (black hollow symbol lines) of round and collapsed armchair (a) and zigzag (b) SWNTs. (c) the vdW attractive energy of bilayer graphene with different stacking patterns calculated by the DFT-D2 method, the red line denotes the average vdW energy of different stacking patterns. (d) The vdW energy and total potential energy (ε_P) of a (30, 15) SWNT as a function of MD simulation time and temperature, the short red line denotes the vdW attractive energy at 300 K. The inset shows a snapshot of the collapsed (30, 15) SWNT during MD simulation at 300 K.

stacking and AA stacking graphene layers is only 0.5%). To estimate this error, we calculated the vdW energy of bilayer graphene with different stacking patterns by the Grimme's DFT-D2 method, in which the vdW interaction was properly considered. As shown in Figure 5c, the vdW interaction between a rotated bilayer graphene is about 10.75% weaker than that for the AB stacked one. Experimentally, most collapsed SWNTs do not have the AB stacking configuration (unless the original SWNT is armchair) and the effective van der Waals interaction should be reduced by 10.75%.

The thermal fluctuation between graphene layers and in collapsed SWNTs can be calculated by the molecular dynamic simulation. As demonstrated in Figure 5d and Figure S10 (Supporting Information), the vdW energy of collapsed SWNTs is a function of temperature. At the normal condition, T = 300 K, the vdW interaction of the bilayer graphene, collapsed (30, 15), and (60, 30) SWNTs are reduced by 1.92, 4.38, and 3.02%, respectively. Considering both (i) and (ii), the vdW interaction of collapsed SWNTs should be approximately reduced by 13% at room temperature. By subtracting the vdW interaction by 13% from the AIREBO potential, the corrected threshold diameter for both armchair and zigzag SWNTs is ~5.1 nm, which is perfectly consistent with the experimental observation.

Next let us consider the formation of round SWNTs larger than 5.1 nm. It is clear that the collapse of a SWNT must experience an energy barrier because of the increasing curvature at the beginning;[16] thus, a rounded SWNT is in a metastable state and therefore the observance of one is not a surprise, but the number of rounded SWNTs must be much less than the number of the collapsed CE-CL-GNRs. In addition, by fitting the results from the calculations, the relationship between the width of the collapsed CE-BL-GNRs and the diameter of the original SWNTs was found to be linear as $W = 1.536 \times D - 0.372$ for armchair SWNTs and $W = 1.531 \times D - 0.393$ for zigzag ones (Figure S11, Supporting Information).

CONCLUSIONS

Individual, free-standing SWNTs with large diameters were grown on calcined 10 nm Au nanoparticles by CVD growth. The inhibition of forming multiwalled carbon nanotubes is attributed to the low carbon solubility in Au particles. Extensive ED characterizations on the Au-grown SWNTs revealed that a number of SWNTs were collapsed to form CE-BL-GNRs. The free-standing CE-BL-GNRs could have different stacking orders, the stability of which was attributed to the restriction of interlayer sliding along the axial direction of the parent SWNTs. In addition, our experiment unambiguously determined that the threshold diameter for SWNTs to collapse, D_T, is 5.1 nm. This value is in agreement with the calculation result implemented by

the classical AIREBO force field and DFT. This work set a new guideline for large-scale synthesis of CE-BL-GNRs *via* spontaneous collapse of SWNTs with large diameters, which would be of great interest to both fundamental graphene/carbon nanotube research and practical applications in graphene nanoribbon-based nanoelectronics.

METHODS

CVD Growth and Characterizations of SWNTs. The Au nanoparticles (10 nm) were supplied by Aldrich (CAS: 752584). A drop of as-received Au particle dispersion was dispersed onto a Si_3N_4 TEM grid (DuraSiN mesh). The catalyst was loaded into a horizontal CVD reactor and annealed in air at 800 °C for 2 h. After that, a flow of 200 cm^3/min helium (He) was introduced while increasing the temperature to 950 °C. Once reaching the desired temperature, the He flow was replaced by methane with a flow rate of 200 cm^3/min, and the growth period lasted for 1 h. After the growth process, the system was finally cooled down under the protection of He. TEM studies were performed using a JEOL-2200FS double aberration-corrected TEM operated at 80 kV. The (*n*, *m*) determination from ED patterns of individual SWNTs was based on a calibration-free intrinsic layer line-spacing method.[34]

Calculation Methods. Adaptive intermolecular reactive empirical bond order potential[40] is used to perform the geometry optimization and MD of SWNTs. The well-depth and equilibrium distance of the Lennard-Jones 12−6 potential are set to be 2.84372 meV and 3.4 Å, respectively. The cutoff distance of the long-range interaction is set to be 10.7 Å. In the geometry optimization, a periodic boundary condition is adopted. A unit cell of 8.520 and 9.838 Å in length along the axial direction of zigzag and armchair SWNTs is used, respectively. Sufficient space (>20 Å) in the radial direction is set to eliminate periodic image interactions. Both the unit cell and the atom coordinates were optimized until the force on each atom is smaller than 10^{-3} eV/Å or the total energy has a tolerance of 10^{-5} eV. In the molecular dynamic calculation, the NVT ensemble is adopted with a time step of 0.1 fs. The unit cells of the (30, 15) SWNT and the (60, 30) SWNT are set to be 200 × 200 × 112.7091 $Å^3$ containing 4200 and 8400 atoms, respectively. The unit cell of bilayer graphene is 20 × 75.9591 × 82.8374 $Å^3$ containing 4896 atoms. (To account for the negative thermal expansion coefficiency of graphene,[41] the unit cell has been shrunk by 1% from the standard one.) At each heating stage, the system temperature is increased by 1 K every 200 MD steps. After the heating process, the system is relaxed for 9 ps to get equilibrium.

For the calculation of the curvature energy of SWNTs, the second generation reactive empirical bond order (REBO) potential[41] is also used for a comparison purpose.

All DFT calculations are implemented using the Vienna ab Initio Simulation Package (VASP).[42] The exchange−correlation potentials are treated by the generalized gradient approximation (GGA) parametrized by Perdew, Burke, and Ernzerhof (PBE).[43] The interaction between valence electrons and ion cores is described by the projected augmented wave (PAW) method. To describe the interlayer graphene interaction exactly, the more accurate DFT-D2 method[44] taking account of vdW interaction was adopted to treat the long-range interatomic interactions. Moreover, to distinguish the local interactions of these two graphene layers, different stacking styles, such as AA, AB, and many other stacking styles with different rotational angles varying from 0 degree (AA stacking) to 60 degree (AB stacking) are examined. The lattice parameters of these bilayer graphenes are set from 2.46 Å (AA, AB stacking) to 24.228 Å according to the different rotation angles between them, and the vacuum layer is set as large as 18 Å. The atoms in the periodic unit are allowed to fully relax, and the reciprocal space is sampled by 9 × 9 × 1 or 1 × 1 × 1 grid meshes using the Monkhorst−Pack scheme[45] according to the different lattice parameters previously discussed.

The interaction energies of these bilayer graphenes are defined as $\varepsilon_{vdW} = (E_{BLG} - 2E_{SLG})/N$, where E_{BLG} and E_{SLG} are the energy of a bilayer graphene at a different rotation angle and the energy of a single layer graphene accordingly. *N* is the number of carbon atoms of one layer of graphene.

The curvature energy (ε_C) of SWNTs obtained from the DFT and REBO method is defined as $\varepsilon_C = E_{SWNT}/N - \varepsilon_G$, where E_{SWNT} is the total energy of the SWNT, ε_G is the energy of a carbon atom in a single layer graphene, and *N* is the number of carbon atoms of the SWNT.

The curvature energy (ε_C) of SWNTs obtained from the AIREBO method is defined as$\varepsilon_C = (E_{SWNT} - E_{vdW})/N - (\varepsilon_G - \varepsilon_{vdW})$, where E_{SWNT} and E_{vdW} are the total energy and the vdW energy of the SWNT, respectively, ε_G and ε_{vdW} are the total energy and the vdW energy of a carbon atom in single layer graphene, and *N* is the number of carbon atoms of the SWNT.

Conflict of Interest: The authors declare no competing financial interest.

Supporting Information Available: Further experimental details and supportive data as described in the text. This material is available free of charge *via* the Internet at http://pubs.acs.org.

Acknowledgment. This work was supported by the CNB-E Project in Aalto University through the Multidisciplinary Institute of Digitalization and Energy (MIDE) program. This work made use of the Aalto University Nanomicroscopy Center (Aalto-NMC) premises.

REFERENCES AND NOTES

1. Motta, M.; Moisala, A.; Kinloch, I. A.; Windle, A. H. High Performance Fibres from 'Dog Bone' Carbon Nanotubes. *Adv. Mater.* **2007**, *19*, 3721–3726.
2. Zhang, C. G.; Bets, K.; Lee, S. S.; Sun, Z. Z.; Mirri, F.; Colvin, V. L.; Yakobson, B. I.; Tour, J. M.; Hauge, R. H. Closed-Edged Graphene Nanoribbons from Large-Diameter Collapsed Nanotubes. *ACS Nano* **2012**, *6*, 6023–6032.
3. Chopra, N. G.; Benedict, L. X.; Crespi, V. H.; Cohen, M. L.; Louie, S. G.; Zettl, A. Fully Collapsed Carbon Nanotubes. *Nature* **1995**, *377*, 135–138.
4. Xiao, J.; Liu, B.; Huang, Y.; Zuo, J.; Hwang, K. C.; Yu, M. F. Collapse and Stability of Single- and Multi-Wall Carbon Nanotubes. *Nanotechnology* **2007**, *18*, 395703.
5. Zhong, X. H.; Wang, R.; Liu, L. B.; Kang, M.; Wen, Y. Y.; Hou, F.; Feng, J. M.; Li, Y. L. Structures and Characterizations of Bundles of Collapsed Double-Walled Carbon Nanotubes. *Nanotechnology* **2012**, *23*, 505712.
6. Yu, M. F.; Kowalewski, T.; Ruoff, R. S. Investigation of the Radial Deformability of Individual Carbon Nanotubes under Controlled Indentation Force. *Phys. Rev. Lett.* **2000**, *85*, 1456–1459.
7. Vilatela, J. J.; Deng, L.; Kinloch, I. A.; Young, R. J.; Windle, A. H. Structure of and Stress Transfer in fibres Spun from Carbon Nanotubes Produced by Chemical Vapour Deposition. *Carbon* **2011**, *49*, 4149–4158.
8. Senga, R.; Hirahara, K.; Nakayama, Y. Nanotorsional Actuator Using Transition between Flattened and Tubular States in Carbon Nanotubes. *Appl. Phys. Lett.* **2012**, *100*, 083110.
9. Choi, D. H.; Wang, Q.; Azuma, Y.; Majima, Y.; Warner, J. H.; Miyata, Y.; Shinohara, H.; Kitaura, R. Fabrication and Characterization of Fully Flattened Carbon Nanotubes: A New Graphene Nanoribbon Analogue. *Sci. Rep.* **2013**, *3*, 1617.
10. Liu, Z.; Suenaga, K.; Harris, P. J. F.; Iijima, S. Open and Closed Edges of Graphene Layers. *Phys. Rev. Lett.* **2009**, *102*, 015501.
11. Liu, H. J.; Cho, K. J. A Molecular Dynamics Study of Round and Flattened Carbon Nanotube Structures. *Appl. Phys. Lett.* **2004**, *85*, 807–809.

12. Tang, T.; Jagota, A.; Hui, C. Y.; Glassmaker, N. J. Collapse of Single-Walled Carbon Nanotubes. *J. Appl. Phys.* **2005**, *97*, 074310.
13. Chang, T.; Guo, Z. Temperature-Induced Reversible Dominoes in Carbon Nanotubes. *Nano Lett.* **2010**, *10*, 3490–3493.
14. Li, Y. Edge-Closed Graphene Nanoribbons Fabricated by Spontaneous Collapse of Few-Walled Carbon Nanotubes. *Phys. Chem. Chem. Phys.* **2014**, *16*, 1921–1929.
15. Liu, B.; Yu, M. F.; Huang, Y. G. Role of Lattice Registry in the Full Collapse and Twist Formation of Carbon Nanotubes. *Phys. Rev. B* **2004**, *70*, 161402.
16. Zhang, S. L.; Khare, R.; Belytschko, T.; Hsia, K. J.; Mielke, S. L.; Schatz, G. C. Transition States and Minimum Energy Pathways for the Collapse of Carbon Nanotubes. *Phys. Rev. B* **2006**, *73*, 075423.
17. Elliott, J. A.; Sandler, J. K. W.; Windle, A. H.; Young, R. J.; Shaffer, M. S. P. Collapse of Single-Wall Carbon Nanotubes Is Diameter Dependent. *Phys. Rev. Lett.* **2004**, *92*, 095501.
18. Harutyunyan, A. R.; Chen, G.; Paronyan, T. M.; Pigos, E. M.; Kuznetsov, O. A.; Hewaparakrama, K.; Kim, S. M.; Zakharov, D.; Stach, E. A.; Sumanasekera, G. U. Preferential Growth of Single-Walled Carbon Nanotubes with Metallic Conductivity. *Science* **2009**, *326*, 116–120.
19. He, M.; Jiang, H.; Liu, B.; Fedotov, P. V.; Chernov, A. I.; Obraztsova, E. D.; Cavalca, F.; Wagner, J. B.; Hansen, T. W.; Anoshkin, I. V.; *et al*. Chiral-Selective Growth of Single-Walled Carbon Nanotubes on Lattice-Mismatched Epitaxial Cobalt Nanoparticles. *Sci. Rep.* **2013**, *3*, 1460.
20. Han, Z. J.; Ostrikov, K. Uniform, Dense Arrays of Vertically Aligned, Large-Diameter Single-Walled Carbon Nanotubes. *J. Am. Chem. Soc.* **2012**, *134*, 6018–6024.
21. Zhou, W.; Ding, L.; Yang, S.; Liu, J. Synthesis of High-Density, Large-Diameter, and Aligned Single-Walled Carbon Nanotubes by Multiple-Cycle Growth Methods. *ACS Nano* **2011**, *5*, 3849–3857.
22. Yu, B.; Liu, C.; Hou, P. X.; Tian, Y.; Li, S.; Liu, B.; Li, F.; Kauppinen, E. I.; Cheng, H. M. Bulk Synthesis of Large Diameter Semiconducting Single-Walled Carbon Nanotubes by Oxygen-Assisted Floating Catalyst Chemical Vapor Deposition. *J. Am. Chem. Soc.* **2011**, *133*, 5232–5235.
23. Cheung, C. L.; Kurtz, A.; Park, H.; Lieber, C. M. Diameter-Controlled Synthesis of Carbon Nanotubes. *J. Phys. Chem. B* **2002**, *106*, 2429–2433.
24. He, M.; Jiang, H.; Kauppinen, E. I.; Lehtonen, J. Diameter and Chiral Angle Distribution Dependencies on the Carbon Precursors in Surface-Grown Single-Walled Carbon Nanotubes. *Nanoscale* **2012**, *4*, 7394–7398.
25. Kiang, C. H. Growth of Large-Diameter Single-Walled Carbon Nanotubes. *J. Phys. Chem. A* **2000**, *104*, 2454–2456.
26. Ci, L.; Vajtai, R.; Ajayan, P. M. Vertically Aligned Large-Diameter Double-Walled Carbon Nanotube Arrays Having Ultralow Density. *J. Phys. Chem. C* **2007**, *111*, 9077–9080.
27. Alvarez, N. T.; Li, F.; Pint, C. L.; Mayo, J. T.; Fisher, E. Z.; Tour, J. M.; Colvin, V. L.; Hauge, R. H. Uniform Large Diameter Carbon Nanotubes in Vertical Arrays from Premade Near-Monodisperse Nanoparticles. *Chem. Mater.* **2011**, *23*, 3466–3475.
28. Yan, K. Y.; Xue, Q. Z.; Zheng, Q. B.; Xia, D.; Chen, H. J.; Xie, J. Radial Collapse of Single-Walled Carbon Nanotubes Induced by the Cu_2O Surface. *J. Phys. Chem. C* **2009**, *113*, 3120–3126.
29. Bernholc, J.; Brabec, C.; Buongiorno Nardelli, M.; Maiti, A.; Roland, C.; Yakobson, B. I. Theory of Growth and Mechanical Properties of Nanotubes. *Appl. Phys. A: Mater. Sci. Process.* **1998**, *67*, 39–46.
30. Rakhmanov, A. L.; Rozhkov, A. V.; Sboychakov, A. O.; Nori, F. Instabilities of the AA-Stacked Graphene Bilayer. *Phys. Rev. Lett.* **2012**, *109*, 206801.
31. Young, N. P.; van Huis, M. A.; Zandbergen, H. W.; Xu, H.; Kirkland, A. I. Transformations of Gold Nanoparticles Investigated Using Variable Temperature High-Resolution Transmission Electron Microscopy. *Ultramicroscopy* **2010**, *110*, 506–516.
32. Takagi, D.; Homma, Y.; Hibino, H.; Suzuki, S.; Kobayashi, Y. Single-Walled Carbon Nanotube Growth from Highly Activated Metal Nanoparticles. *Nano Lett.* **2006**, *6*, 2642–2645.
33. Takagi, D.; Kobayashi, Y.; Hlbirio, H.; Suzuki, S.; Homma, Y. Mechanism of Gold-Catalyzed Carbon Material Growth. *Nano Lett.* **2008**, *8*, 832–835.
34. Jiang, H.; Nasibulin, A.; Brown, D.; Kauppinen, E. Unambiguous Atomic Structural Determination of Single-Walled Carbon Nanotubes by Electron Diffraction. *Carbon* **2007**, *45*, 662–667.
35. Jiang, H.; Brown, D.; Nasibulin, A.; Kauppinen, E. Robust Bessel-Function-Based Method for Determination of the (N,M) Indices of Single-Walled Carbon Nanotubes by Electron Diffraction. *Phys. Rev. B* **2006**, *74*, 035427.
36. Qin, L. C. Determination of the Chiral Indices (*n*, *m*) of Carbon Nanotubes by Electron Diffraction. *Phys. Chem. Chem. Phys.* **2007**, *9*, 31–48.
37. Huang, J. Y.; Chen, S.; Ren, Z. F.; Wang, Z. Q.; Wang, D. Z.; Vaziri, M.; Suo, Z.; Chen, G.; Dresselhaus, M. S. Kink Formation and Motion in Carbon Nanotubes at High Temperatures. *Phys. Rev. Lett.* **2006**, *97*, 075501.
38. Hernandez, Y.; Nicolosi, V.; Lotya, M.; Blighe, F. M.; Sun, Z. Y.; De, S.; McGovern, I. T.; Holland, B.; Byrne, M.; Gun'ko, Y. K.; *et al*. High-Yield Production of Graphene by Liquid-Phase Exfoliation of Graphite. *Nat. Nanotechnol.* **2008**, *3*, 563–568.
39. Brown, L.; Hovden, R.; Huang, P.; Wojcik, M.; Muller, D. A.; Park, J. Twinning and Twisting of Tri- and Bilayer Graphene. *Nano Lett.* **2012**, *12*, 1609–1615.
40. Stuart, S. J.; Tutein, A. B.; Harrison, J. A. A Reactive Potential for Hydrocarbons with Intermolecular Interactions. *J. Chem. Phys.* **2000**, *112*, 6472–6486.
41. Yoon, D.; Son, Y. W.; Cheong, H. Negative Thermal Expansion Coefficient of Graphene Measured by Raman Spectroscopy. *Nano Lett.* **2011**, *11*, 3227–3231.
42. Kresse, G.; Furthmuller, J. Efficient Iterative Schemes for ab Initio Total-Energy Calculations Using a Plane-Wave Basis Set. *Phys. Rev. B* **1996**, *54*, 11169–11186.
43. Perdew, J. P.; Burke, K.; Ernzerhof, M. Generalized Gradient Approximation Made Simple. *Phys. Rev. Lett.* **1996**, *77*, 3865–3868.
44. Grimme, S. Semiempirical GGA-Type Density Functional Constructed with a Long-Range Dispersion Correction. *J. Comput. Chem.* **2006**, *27*, 1787–1799.
45. Monkhorst, H. J.; Pack, J. D. Special Points for Brillouin-Zone Integrations. *Phys. Rev. B* **1976**, *13*, 5188–5192.